

A method based on a dual frequency resonator to estimate physical parameters of superconductors from surface impedance measurements in a magnetic field

Nicola Pompeo^{a,*}, Kostiantyn Torokhtii^a, Andrea Alimenti^a, Enrico Silva^a

^a*Dipartimento di Ingegneria, Università Roma Tre, Via Vito Volterra 62, 00146 Rome, Italy*

Abstract

High frequency applications of superconductors in a dc magnetic field rely on the estimate of the characteristic crossover frequency ν_c between low and high losses. Customarily, high sensitivity resonant techniques, intrinsically operating at discrete frequencies, are used to estimate ν_c . We exploit here a method based on a dual frequency resonator. We show that single-frequency evaluations of ν_c lead to heavy underestimations of the superconductor surface resistance. We describe a combined analytical and experimental approach that gives more accurate estimates for ν_c , and additionally allows to test the underlying physical model.

Keywords: Dielectric Resonators, Superconductors, Surface Impedance, Microwave Measurements, Multifrequency.

1. Introduction

Cutting edge fundamental research fields relies heavily on the low losses of superconductors at radio and microwave frequencies. As a first example, particle accelerators require superconducting cavities [1, 2] in which the extremely low losses allow for high cavity quality factor Q , and then strong accelerating electric fields of the order of tens of MV/m. The power handling capabilities of the next generation particle accelerators will be so demanding that also the beam screens, necessary to confine the synchrotron radiation emitted by the charged, high-energy particles over their bent trajectories are thought to require superconductors: the entire length of the 100-km long beam tunnel of the Future Circular Collider (FCC) could be covered by a suitable superconductor. As a striking difference with respect to well-established applications of high-frequency superconductivity, the superconductors should keep the losses much lower than those of copper at frequencies up to ~ 2 GHz

in very intense static magnetic fields at the scale of 16 T [3, 4]. A similar requirement – superconductors operating at microwave frequencies in a dc field of several tesla – is shared by dark matter hunting experiments: axions, possible candidates for the elusive dark matter, are predicted to interact with the electromagnetic field of high Q resonators, tuned to their mass frequency equivalent, within static magnetic fields, so that setups with superconducting cavities have been designed and tested [5, 6]. The sensitivity of the instrument is proportional to $Q \cdot B^2$, where B is the magnetic flux density, so it is clear that low losses and high dc fields are requested. The physical quantity determining the electromagnetic response of a conductor (and of a superconductor) in the high frequency regime is the surface impedance Z . This is a complex quantity, defined as $Z := E_t/H_t$, ratio of the tangential components of the electric E_t and magnetic H_t field on the superconductor surface [7, §2.6][8, §87][9, §8.1]. Hence, the prediction, determination and optimization of the surface impedance Z of superconductors, and in particular of the surface resistance $R := \text{Re}(Z)$ which governs the power losses [7, §2.9, §7.4][9, §8.1], are of renewed and paramount relevance. The expression $Z = \sqrt{i2\pi\nu\mu_0\rho}$ connects the complex resistivity

*Corresponding author.

Email: nicola.pompeo@uniroma3.it.

<https://doi.org/10.1016/j.measurement.2021.109937>.

Available online 29 July 2021.

Distributed under CC-BY-NC-ND license.

(material property) ρ to Z [7] at the frequency ν (μ_0 is the magnetic permeability) in (super)conductors with thickness d larger than the normal δ and London λ penetration depths [10]. In a static magnetic field, however, the losses in the ubiquitously used type II superconductors are dominated by far by the motion of quantized flux tubes ("fluxons" or "vortices") [11]. Fluxons oscillate under the Lorentz force exerted by the high frequency currents, giving rise to electrical fields with components parallel to the currents, thus yielding power dissipation. Their motion is hindered by material defects that "pin" the vortices, exerting an elastic recall. The beneficial (from the point of view of limited power dissipation) effect of pins can be weakened by thermal activating depinning (often referred to as fluxon creep).

The widely accepted model [11] describes fluxons under a high frequency current as damped harmonic oscillators, with an additional stochastic thermal force [12, 13]. The resulting expression for the complex vortex motion resistivity ρ_v can be written down as [14]:

$$\rho_v = \rho_{ff} \frac{\chi + i \frac{\nu}{\nu_c}}{1 + i \frac{\nu}{\nu_c}} = \rho_{v1} + i \rho_{v2} \quad (1)$$

where $\rho_{ff} \propto B$ [11] is the so-called flux flow resistivity, corresponding to the fluxon motion free from pinning and thermal activation; $\chi \in [0, 1]$ is an adimensional creep factor, mapping absent to total thermal activation; ν_c is a characteristic frequency, depending on χ and on the so-called (de)pinning frequency ν_p through a function which depends on the specific model used [14]. The latter equality defines the real and imaginary parts of ρ_v . At zero creep, $\nu_c \rightarrow \nu_p$.

Figure 1 reports ρ_v , Eq. (1), at a fixed field and temperature and as a function of the frequency. The role of the various parameters is graphically depicted. ρ_{ff} and $\rho_{ff}\chi$ set the upper limit and the lower limit of the real resistivity, respectively, and the characteristic frequency ν_c marks the crossover between the low-frequency, low dissipation from the high-frequency, high dissipation regime. As such, ν_c or the zero-creep limit ν_p are often used to synthetically describe the performances of a superconductor for high frequency applications. Remarkably, very little studies exist in very high dc field microwave superconductivity, and the applied methods usually rely on older models [15] with $\chi = 0$. The latter is a questionable choice for high- T_c superconductors:

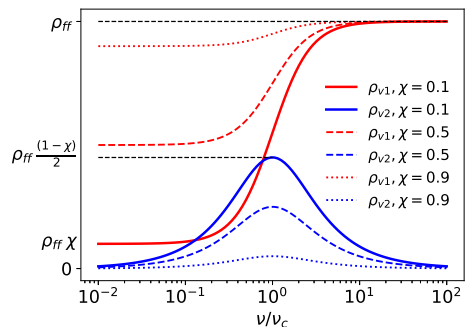


Fig. 1. Frequency dependence of the real and imaginary parts of ρ_v , Eq. (1), plotted for $\chi = \{0.1, 0.5, 0.9\}$.

their high operating temperature ($T_c \sim 30 - 100$ K) and their layered microscopic structure, make the thermal effects much more effective than in low- T_c ($T_c \sim 1 - 10$ K), isotropic superconductors. Moreover, when accurate measurements are performed, even in the latter the thermal effects can be detected [16, 17]. This paper describes a method to accurately measure all the three relevant vortex parameters.

Wideband (i.e. over more than a decade in frequency), swept-frequency measurements are the first obvious choice to test Eq. (1) and to derive the vortex parameters. Although the cryomagnetic environment severely limits the accuracy of such techniques [18], a few attempts were successful in particular with the so-called Corbino disk technique [18–21].

Low sensitivity and difficult calibration (in a cryogenic environment) relegate the wideband techniques to niche studies, in favour of the more sensitive and widely used resonator-based methods [22–34]. The latter have been also codified as an International Standard [35] for what concerns the high sensitivity measurement of R in zero magnetic field only.

Resonators work intrinsically at fixed frequencies dictated by the resonant mode of operation. Two observables can be measured, the real and imaginary part of ρ_v , against three parameters. The common approach neglects χ altogether. Although estimates for ρ_{ff} and ν_p can still be given, it can be shown that the associated uncertainties can reach and exceed 100% [14].

Multi-mode resonators, capable of operating at multiple discrete frequencies, can be a viable al-

ternative [22, 36]. In superconductors, planar resonators are typically exploited, with the need for thin film, patterned in the needed geometry.

Here we propose the exploitation of a purpose-built dual mode Hakki-Coleman [37] dielectric loaded resonator, operating on two quasi-transverse electric (TE) modes with spaced resonant frequencies ~ 16 GHz and ~ 27 GHz. Surface perturbation method is employed, to allow for the measurement of pristine samples. The aim is the determination of all the main vortex parameters, in particular the characteristic frequency ν_c redbut including also the often neglected creep factor, of superconducting thin films. A suitable method for their extraction from dual frequency measurement is presented, with an emphasis on the uncertainty evaluation and their minimization by suitably selecting the measuring frequencies. Preliminary results were reported in Ref. [38].

The paper is organized as follows. In Sec. II the measurement technique is briefly described, providing the necessary background. In Sec. 3 we discuss the data analysis method, including the optimization of the uncertainties on the vortex parameters derived by dual frequency measurements. Sample measurements and results are reported in Sec. 4. Short conclusions are drawn in Sec. 5.

2. The measurement technique

Surface impedance measurements are performed by means of a copper cylindrical electromagnetic resonator, loaded with a single crystal sapphire rod (diameter 7.13(1) mm, height 4.50(1) mm), as reported in Fig. 2. The dielectric-loaded res-

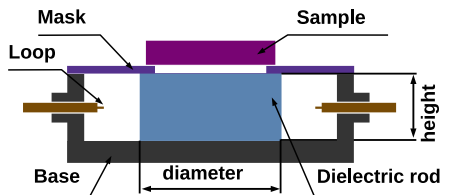


Fig. 2. Sketch of the dielectric resonator. The coupling is made through loops laying on the plane normal to the section plane here depicted, in order to couple with the magnetic field lines.

onator (DR) design process has been a standard one: we have built up a mode chart by means of finite-element electromagnetic numerical simulations with commercially available software, we have

optimized the dielectric rod size to obtain (i) good frequency separation of the desired modes from the unwanted ones, (ii) high Q , (iii) high sensitivity for samples of typical size 10×10 mm², with the constraints given by our measurement apparatus, in which the cryostat has to be placed inside a magnet. For additional information about the design process and accuracy matters we refer to specialized papers [34, 40], together with Ref. [27] as an excellent example about standard steps in the design. The resonator is used in the end-wall replacement configuration with samples of size ~ 1 cm² placed on a base and covered by a thin metal mask, with a central hole of diameter 6.50(1) mm in order to preserve the circular symmetry of the structure. The resonator operates on the quasi-transverse electric TE_{0l1} ($l = 1, 2$) modes, with resonant frequencies $\nu_{res,1} = 16.4$ GHz and $\nu_{res,2} = 26.6$ GHz. The operating frequencies are chosen in view of the applications and the reasonably easy interpretation of the data. Applications, such as the mentioned FCC beam screen, require a characteristic frequency in the range of tens of GHz. Thus, it is appropriate to experimentally probe a range close to the desired values in order to have maximum sensitivity. Second, the frequency needs to be kept sufficiently high so that the fluxon motion is limited to tiny oscillations, a requirement for Eq. 1 whence the fluxon parameters.

The external microwave line is coupled to the resonator by means of loop antennas. The resonator is operated in transmission, and the two-ports scattering coefficients S_{ij} ($i, j = 1, 2$) are measured by a Vector Network Analyzer, with frequency sweeps around each of the resonant frequencies.

The cryogenic environment prevents a full calibration. The uncalibrated sections of the transmission lines and other non-idealities were taken into account by the fit procedure [40, 41], in order to measure the quality factor Q of the resonator and the resonant frequency ν_{res} for each mode.

Since from now on we focus on magnetic field H induced variations, in the following, for a generic physical quantity A , $A(H)$ denotes its value for the value H of the magnetic field, $A(0) = A(H = 0)$ and:

$$\Delta A(H) := A(H) - A(0) \quad (2)$$

To derive the vortex parameters, the field variation of the surface impedance $\Delta Z(H) = \Delta R(H) + i\Delta X(H)$ – where $X := \text{Im}(Z)$ denotes the surface reactance – at fixed temperature T is needed.

Within the small perturbation approach, the superconducting sample contributes to the DR Q and resonant frequency shift $\Delta\nu_{res}$ through [42]:

$$R(H) = \frac{G}{Q(H)} - background_R \quad (3a)$$

$$\Delta X(H) = -2G \frac{\nu_{res}(H) - \nu_{res}(0)}{\nu_{res}(0)} + background_X \quad (3b)$$

where G is a mode-dependent geometrical factor, determined through finite elements electromagnetic simulations, and $background_R$ and $background_X$ are the DR contributions (due to its bases, the mask, the lateral wall and the dielectric rod) to Q and ν_{res} , respectively. Since the DR is made of non-magnetic materials, these quantities yield no/negligible variations by varying the applied magnetic field. Hence, focusing on $\Delta Z(H)$:

$$\Delta R(H) = G \left(\frac{1}{Q(H)} - \frac{1}{Q(0)} \right) =: G\Delta r(H) \quad (4a)$$

$$\Delta X(H) = -2G \frac{\nu_{res}(H) - \nu_{res}(0)}{\nu_{res}(0)} =: G\Delta x(H) \quad (4b)$$

where Δr and Δx are defined through the last equalities in both equations and represent normalized measured quantities, useful for the discussion in Sec. 3.

Examples of actual resonance curves as measured in terms of the scattering coefficient $|S_{21}|$ for both modes are reported in Fig. 3. The resonator is loaded with the superconducting sample described in Sec. 4. Measurements are taken at the fixed temperature $T = 10.00(5)$ K and at selected applied magnetic field intensities. The changes of Q and ν_{res} with the applied field reflect the changes in Z due to the motion of flux lines, according to Eq. (4). The field dependent $Q(H)$ and $\nu_{res}(H)$ for the two modes are reported in Fig. 4, where is apparent the magnitude of the superconductor surface impedance field induced variations with respect the absolute values of Q and ν_{res} . Finally, the obtained resonant frequencies are well in agreement with those computed through finite element electromagnetic simulations, thus allowing a clear identification. In films of thickness $d \ll \min(\delta, \lambda)$ the so-called thin-film approximation applies [10]:

$$\Delta Z(H) \simeq \frac{\rho_v(B)}{d} \quad (5)$$

with $B \simeq \mu_0 H$ in the London limit.

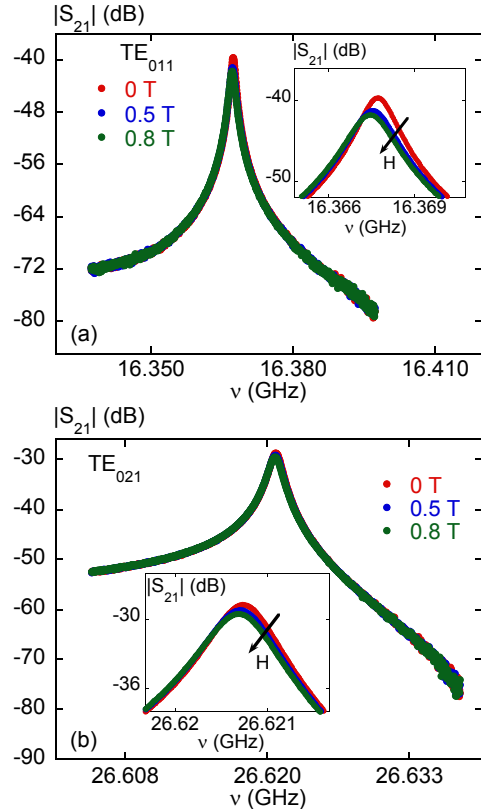


Fig. 3. Modulus of the scattering coefficient S_{21} of the resonator vs ν around the resonant frequencies of the two modes (TE_{011} in panel (a), TE_{021} in panel (b)), measured at fixed $T = 10.00(5)$ K and at elected magnetic fields H . The change in the resonator response due to the sample $Z(H)$ is apparent. In the insets, zooms of the curves.

3. Method

3.1. General aspects

The complex vortex motion resistivity ρ_v is obtained at the frequencies $\nu_{res,i}$, (with $i = \{1, 2\}$ referring to the first TE_{011} and second (TE_{021}) resonant mode, respectively) by combining measurements of Q_i and $\nu_{res,i}$ at fixed T and variable H (Eq. (4)), with the thin film approximation Eq. (5), to get:

$$\begin{aligned} \rho_{v,i} &= \rho_{v1,i} + i\rho_{v2,i} = \\ &= G_i d \left[\Delta \frac{1}{Q_i} + i \left(-2 \frac{\Delta \nu_{res,i}}{\nu_{res,i}} \right) \right] = \\ &= G_i d (\Delta r_i + i\Delta x_i) \end{aligned} \quad (6)$$

where Δ denotes the field variations as in Eq. (2), $\rho_{v1} := \text{Re}(\rho_v)$ and $\rho_{v2} := \text{Im}(\rho_v)$. In Eq. (6) only

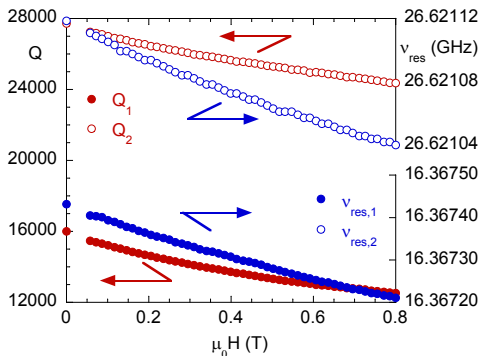


Fig. 4. Field dependent $Q_i(H)$ and $\nu_{res,i}(H)$, with $i = \{1, 2\}$ for TE_{011} and TE_{021} resonant mode, respectively, measured at fixed $T = 10.00(5)$ K. The change in the resonator response due to the sample $Z(H)$ is apparent.

experimental quantities are present. Once ρ_v is obtained from measurements, vortex parameters are obtained within the model of Eq. (1). An important point is the evaluation of the uncertainties involved. In this paper, standard deviations are used to evaluate the uncertainties (coverage factor $k = 1$).

Before addressing the possible methods to obtain the vortex parameters, in particular ν_c , it is useful to recall some features of the theoretical model.

Fig. 1 reports a plot of the real and imaginary parts of ρ_v vs ν (note the logarithmic scale for the frequency) for selected values of $\chi = \{0.1, 0.5, 0.9\}$. The real part increases monotonously, from a low frequency value $\rho_{ff}\chi$ to the asymptotic high frequency limit ρ_{ff} ; the imaginary part is vanishingly small in the above two limits (hence, from a measurement point of view this implies a small measurable signal) and attains a maximum value $\rho_{ff}(1 - \chi)/2$ at ν_c . By increasing the creep factor χ from 0 to 1 (physically, with increased thermal processes), the above features wash out, ultimately yielding constant $\rho_{v1} \rightarrow \rho_{ff}$ and $\rho_{v2} \rightarrow 0$ and preventing a precise determination of ν_c . Since the focus is on the accurate determination of ν_c , one should carefully choose the measuring frequencies ν_i , given by the resonant frequencies $\nu_{res,i}$ of the DR. By focusing the attention on the real part only, one would expect a maximum sensitivity to ν_c through measurements on the maximum slope of ρ_{v1} , with a choice $\nu_1 < \nu_c < \nu_2$, and ν_i sufficiently separated and not too far from ν_c . It will be clear later that this is not the only good choice

from the point of view of reduced uncertainties.

We describe now two main approaches to the determination of the vortex parameters: standard multiple curve fitting and a closed-form, analytical solution by inversion of Eq. (6). We show below that the closed-form approach leads, in some circumstances, to lower uncertainties than a plain fitting. Moreover, it can be used to optimize the technique by determining the best choice of the measurement frequencies to minimize the uncertainty on the most important quantity, ν_c .¹ Finally, a combination of the methods can help to shed light on the consistency of the model with the experimental data.

3.2. Standard curve fitting

The standard curve fitting, based on the non-linear least squares Levenberg-Marquardt algorithm [43, 44], fits at each H, T the four experimental points $\rho_{v1}(\nu_1), \rho_{v2}(\nu_1), \rho_{v1}(\nu_2), \rho_{v2}(\nu_2)$ to the theoretical Eq. (1). Its outputs are the fit parameters (ν_c, χ and ρ_{ff}) with their uncertainties, determined from the covariance matrix of the fit parameters. We refer to this approach as “agnostic”: it is applied without exploiting any particular mathematical properties of Eq. (1) or physical properties of the underlying model. Moreover, the adherence of the data to the model is neither questioned nor checked. Indeed, inconsistencies of the data with the theoretical model do not emerge from the fit procedure, that provides the fitting parameters anyway, possibly with increased uncertainties. We further comment on this point in Sec. 3.4.

3.3. Closed form inversion: ν_c and χ

The analytical solution in closed form can be computed from the overdetermined system of four equations obtained by equating the measurements at the two frequencies of the real and imaginary parts of ρ_v , four observables, to Eq. (1), containing

¹It is worth noting that the ratio between the measurement frequencies cannot be completely freely chosen, because of the constraints related to the actual resonators and modes that can be used, so that an indication of a range of acceptable values for ν_i , around the optimal values, is necessary.

the three unknowns (ν_c , χ and ρ_{ff}):

$$\rho_{ff} \frac{\chi + \left(\frac{\nu_1}{\nu_c}\right)^2}{1 + \left(\frac{\nu_1}{\nu_c}\right)^2} = G_1 d \Delta r_1 \quad (7a)$$

$$\rho_{ff} \frac{(1 - \chi) \frac{\nu_1}{\nu_c}}{1 + \left(\frac{\nu_1}{\nu_c}\right)^2} = G_1 d \Delta x_1 \quad (7b)$$

$$\rho_{ff} \frac{\chi + \left(\frac{\nu_2}{\nu_c}\right)^2}{1 + \left(\frac{\nu_2}{\nu_c}\right)^2} = G_2 d \Delta r_2 \quad (7c)$$

$$\rho_{ff} \frac{(1 - \chi) \frac{\nu_2}{\nu_c}}{1 + \left(\frac{\nu_2}{\nu_c}\right)^2} = G_2 d \Delta x_2 \quad (7d)$$

In the above, the subscripts $i = \{1, 2\}$ in the quantities Δr_i , Δx_i , G_i , similarly to what already done for ν_i , indicate the first (TE₀₁₁) and second (TE₀₂₁) resonant mode, respectively. Here the measuring frequencies ν_i correspond to $\nu_{res,i}$ in the experiment. In the following computation of the uncertainties on the vortex parameters, $u(\nu_i)$ is the main source of uncertainty on ΔX , but its other contributions to the overall uncertainties on the vortex parameters can be neglected². In order to solve Eq.s (7), it proves helpful to define the following ratio quantities:

$$\bar{r}_1 := \frac{\rho_{v2,1}}{\rho_{v1,1}} = \frac{\Delta x_1}{\Delta r_1} = \frac{\frac{\nu_1}{\nu_c}(1 - \chi)}{\chi + \left(\frac{\nu_1}{\nu_c}\right)^2} \quad (8a)$$

$$\bar{r}_2 := \frac{\rho_{v2,2}}{\rho_{v1,2}} = \frac{\Delta x_2}{\Delta r_2} = \frac{\frac{\nu_2}{\nu_c}(1 - \chi)}{\chi + \left(\frac{\nu_2}{\nu_c}\right)^2} \quad (8b)$$

We stress that the second equality expresses the ratios \bar{r}_i in terms of purely experimental quantities (the geometrical factors G_i and the thickness d cancel out), while the last equality makes the connection with the theoretical expression, Eq. (1), and only two unknowns, ν_c and χ , appear. Thus, Eq.s(8) can be solved providing analytical expressions for $\nu_c(\bar{r}_1, \bar{r}_2)$ and $\chi(\nu_c, \nu_i)$. Explicit expressions are reported and discussed in Appendix A. Analytical constraints allow to establish the range

²Indeed, considering that ν_i is normalized to ν_c , the typical value $u(\nu_i)/\nu_i \sim 10^{-7}$ is negligible with respect to $u(\nu_c)/\nu_c \sim 10^{-2} - 10^{-1}$ which is obtained by taking $u(\nu_i) = 0$ (see later).

of admissible values of \bar{r}_i as:

$$\frac{\bar{r}_1}{p} \leq \bar{r}_2 \leq p \bar{r}_1 \quad (9)$$

where $p := \nu_2/\nu_1 > 1$. This is an important analytical outcome, since it provides a simple experimental test of the applicability of the model, Eq. (1), to the data set. Moreover, on more practical grounds, it allows also to check if the system can be actually solved: in the case of data close to the domain boundaries, the random uncertainties on \bar{r}_i may push the data outside of the allowed domain, preventing the computation of ν_c . Two additional conditions are related to the scale factors. The first is trivial: $\rho_{v1,1} < \rho_{v1,2}$ (see Fig. 1). The second refers directly to the determination of ρ_{ff} , that we address in the next subsection.

3.4. Closed form inversion: determination of ρ_{ff}

Once χ and ν_c are determined by Eq.s (8), ρ_{ff} can be obtained from the remaining two equations from (7). Explicit expressions are given in Sec. Appendix A. Since the problem is overdetermined (two remaining equations, one unknown), the two solutions $\rho_{ff,1}$ and $\rho_{ff,2}$ (that should be equal within the uncertainties) can be compared as a consistency check. If $\rho_{ff,1}$ and $\rho_{ff,2}$ overlap within the uncertainties, the experimental data is fully compatible with the theoretical model, and ρ_{ff} can be taken as their average. Otherwise, either (i) the values of G_i are not correct and/or some uncertainties have been underestimated, thus indicating a revision of the data analysis, or (ii) the experimental data are not compatible with the theoretical prediction of Eq. (1). The latter is a result “*per se*” since the model can and is customarily (e.g. in design processes) used to estimate the expected surface impedance of a superconductor at frequencies different from the measurement ones. It is clear that if in a given superconducting material the model cannot be applied, any extrapolation based on it would not be reliable.

By contrast, the “agnostic” fit-based approach is certainly more robust, apart from possibly larger uncertainties, in that it gives a result anyway, but it cannot provide this important check.

3.5. Optimal choice of the measuring frequencies

From the analytical solutions for ν_c and χ the uncertainties $u(\nu_c)$ and $u(\chi)$ can be easily computed in closed form (see Appendix A). This feature is

helpful in finding the optimum pair of measuring frequencies ν_i which minimizes $u(\nu_c)$. This can be useful both in the design process of a resonator, and to determine which uncertainty to expect with a given resonator. The numerical study takes advantage from working in normalized frequencies, ν_1/ν_c and ν_2/ν_c . To reduce the parameter space to be explored, we take $u(\Delta r_i) = u(\Delta x_i)$, as reasonable in typical real setups. The resulting uncertainty depends also on the combined parameter $s := G_2 u(\Delta r_2)/G_1 u(\Delta r_1)$ (see Appendix A, Eq. (A.4)).

We thus explore the parameter space $\nu_1/\nu_c < \nu_2/\nu_c$ in the range $[0, 5]$ for selected values of χ and s .³ Some results for sample values χ and $s = 2$ are reported in Fig.s 5. The horizon-

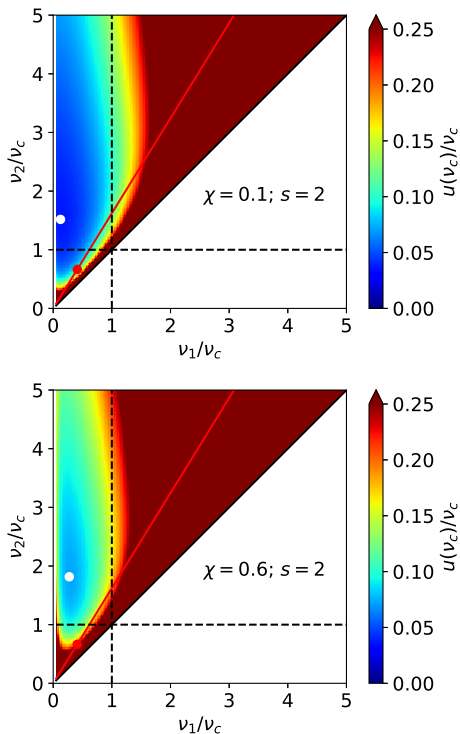


Fig. 5. Relative uncertainty $u(\nu_c)/\nu_c$ vs (ν_1, ν_2) computed for $s = 2$ (value for the resonator described in Sec. 4) and selected values of χ (0.1 and 0.6, upper and lower panel respectively). White area: $\nu_1/\nu_c > \nu_2/\nu_c$, values not computed.

³For the resonator described in Sec. 4, we have $s \simeq 2$. The overall scale factor $u(\Delta r_1)G_1 d/\rho_{ff}$, see Eq. (A.4), is computed for the resonator and the measurement shown in Sec. 4.

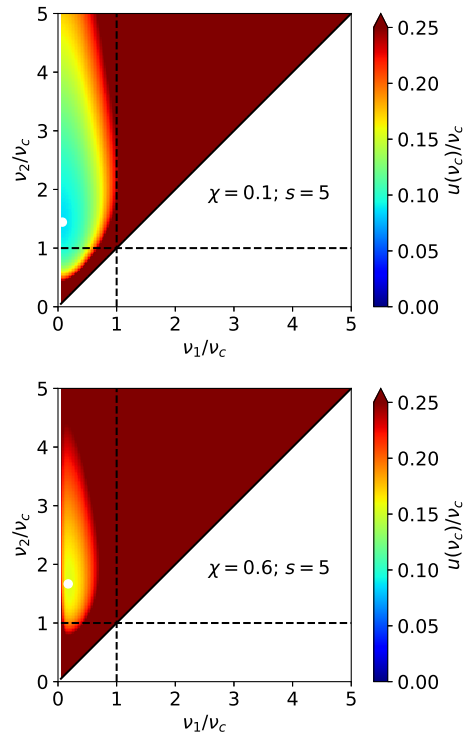


Fig. 6. Relative uncertainty $u(\nu_c)/\nu_c$ vs (ν_1, ν_2) computed for $s = 5$ and selected values of χ (0.1 and 0.6, upper and lower panel respectively).

tal and vertical dashed lines correspond to $\nu_2 = \nu_c$ and $\nu_1 = \nu_c$, respectively. It can be seen that the smaller uncertainties (blue region) are obtained mainly when $\nu_1 < \nu_c$ and $\nu_2 > \nu_c$, as anticipated in Sec. 3.1. An important result is that also $\nu_1 < \nu_c$ and $\nu_2 < \nu_c$ can lead to acceptable uncertainties, depending on the values of χ (higher χ imposes more stringent choices on ν_i). The normalized pair (ν_1, ν_2) corresponding to the absolute minimum uncertainty $u(\nu_c)$ is marked as a white dot, well within the blue region.

The main features are not affected by the values of s and χ : as an example, in Fig. 6 a case with a worst, higher $s = 5$ is presented.

The red continuous lines Fig. 5 represent the working region of the dielectric resonator presented in Sec. 4, where $p = 1.62$. The intersection of this line with yellow region, corresponding to a maximum accepted relative uncertainty $u(\nu_c)/\nu_c \sim 15\%$, yields the range of possible ν_c (in this case 10–60 GHz) which can be determined within the asked uncertainty. The actual working point on this line depends on the ν_c value of an ac-

tual sample: for example, the red point marks the position for the measurement described in the next Section, which yields $\nu_c = 40$ GHz for $\mu_0 H = 0.5$ T.

3.6. Comparison between closed form inversion and fitting approaches

The system of equations (8) does not depend on G_i and d . Thus, in the inversion method $u(\nu_c)$ and $u(\chi)$ are not affected by the uncertainties on these two quantities, and only the evaluation of ρ_{ff} depends on the products $G_i d$.

The ‘‘agnostic’’ fit-based approach, on the other hand, does not exploit the normalized \bar{r}_i and thus is affected by the uncertainties on G_i and d . The thickness d is a common scale factor for all the Δx_i and Δr_i : it does not modify the observed frequency dependence and thus does not impact on ν_c and χ .

The two geometrical factors, however, do not behave as a common scale factor: they affect in different fashions the measured quantities at the different frequencies, yielding an increased uncertainty on ν_c and χ with respect to the analytical inversion approach. Additionally, since they are related to modes sustained by the same resonator, they are affected by the same uncertainties on the dimensions of the resonator and on the permittivity of the dielectric, so that G_1 and G_2 have correlated uncertainties. Obviously, these effects are visible if the uncertainties on G_i are not negligible with respect to those on Δr_i and Δx_i .

It is worth stressing that, while the fit can always be applied so that some values of the vortex parameters can be obtained, the analytical inversion approach requires the strict respect of the condition (9) to extract the vortex parameter.

4. Experimental results and discussion

The measurements are performed at fixed, cryogenic temperature by putting the resonator inside an Oxford Instruments helium-flow CF-Dynamic Cryostat, placed between the polar expansions of a conventional electromagnet Bruker B-E25v. Sample thermalization is obtained by setting the cryostat temperature slightly lower than the desired temperature, through the helium flow and through heaters operated by an Oxford Instruments temperature controller ITC503S, and then by fine controlling resistive heaters mounted on the resonator. The scattering coefficients of the resonator are measured by means of a R&S ZVA-40 VNA, connected

to the resonator through a ~ 1 m long cryogenic and nonmagnetic phosphor-bronze coaxial line plus a ~ 1.5 m long standard coaxial line at room temperature. All coaxial cables have 40 GHz cut-off frequencies and mount K connectors. The desired temperature is reached in zero-field cooling conditions, and then measurements are performed with a magnetic field H applied perpendicularly to the sample surface. The sample used for the present discussion is a nominally $d = 240$ nm thick $\text{FeSe}_{0.5}\text{Te}_{0.5}$ superconductor film, with critical temperature $T_c \sim 18$ K, deposited on a CaF_2 substrate. Further details are reported in [45, 46].

A typical measurement at $T = 10.00(5)$ K is reported in Fig. 7, where ΔZ_1 and ΔZ_2 for the two modes are reported in terms of real and imaginary parts vs the field H . The uncertainties are computed by taking $u(Q_i)/Q_i = 1\%$ and $u(\nu_{res,i})/\nu_{res,i} = 2 \times 10^{-7}$ as dominant uncertainties arising from the partial calibration of the cryogenic measurement line [47]. The relative uncertainties on numerically computed G_i can be typically in the 1% – 8%. With our estimates on the uncertainties of geometrical dimensions and permittivity, we estimate $u(G_i)/G_i = 3\%$. Such figure can improve with very accurate values for the permittivity [48, 49]. The relative uncertainty $u(d)/d$ depends on the technique used for its determination. The determination on the basis of the growth rate of the epitaxial film is typically 10%, while the use of atomic scanning force microscopes [50] yields $\sim 1\%$. Here we take $u(d)/d = 5\%$.

In Fig. 8 we report the vortex parameters extracted through the analytical and fit approaches discussed in the previous Section. It can be seen that in our case $u(G_i)/G_i > u(\Delta r_i)/\Delta r_i, u(\Delta x_i)/\Delta x_i$, so that the analytical inversion approach yields much smaller uncertainties on ν_c and χ , while on the other hand the curve fit provides a smaller $u(\rho_{ff})$.⁴

The obtained results are very sound on physi-

⁴A slight systematic difference between the values obtained with the different methods can be noted. Since this difference is well within the uncertainty bars ($k = 1$), it could seem irrelevant. However, we verified that the two approaches always provide coincident values when tested with numerically simulated data. The slight difference obtained on real data can be considered a further test for the applicability of the model. As an example, wideband measurements on the cuprate superconductor $\text{YBa}_2\text{Cu}_3\text{O}_{7-\delta}$ [51] showed that below $\sim 1 - 4$ GHz, depending on the T and H ranges, the model of Eq. (1) does not apply. The little difference in the results of Fig.8 could be a precursor of a similar effect.

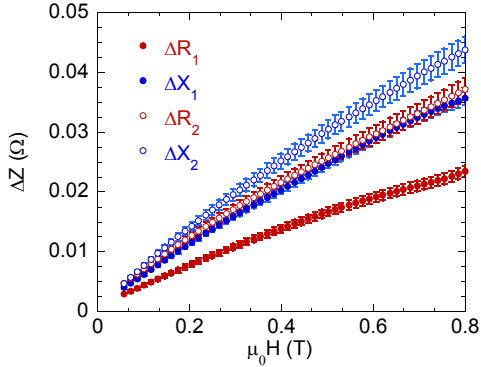


Fig. 7. $\Delta Z_i(H)$ at two frequencies, $\nu_{res,i} = \{16.4, 26.6\}$ GHz, vs field H at fixed $T = 10.00(5)$ K.

cal grounds: ν_c and χ are nearly field independent, while ρ_{ff} is almost linear vs H , thus consistent with general models for the flux flow resistivity [52]. The obtained ν_c is within a factor of 2.5 with respect to values reported in literature for $\nu_c(\chi = 0)$ both in thin films [53] and single crystals [54]: considering the underestimation involved in the assumption $\chi = 0$, as discussed in Sec. 1, together with the differences between distinct samples, this result is not unreasonable and it underlines the need of accurate measurements of the fundamental parameter ν_c . The creep factor, although small, is not negligible even at this low temperature, as often naively assumed: this is consistent with results obtained with wide-band measurements in the same temperature range in other superconductors like Nb [17].

4.1. Comparison with single frequency determinations

It is of interest to compare the characteristic frequency value ν_c , as obtained with the dual frequency (ν_1 and ν_2) method here described, to the value which would be obtained from a single frequency measurement, i.e. $\nu_{p0} := \nu_c(\chi = 0)$ from ν_1 only (as an example). In the latter case, one obtains $\nu_{p0} = 25(1)$ GHz: it can be seen that ν_{p0} is a heavy underestimation of ν_c . Since measurements are often employed to compute values for ρ_v or Z at different frequencies, it is useful to stress that the significant underestimate inherent in ν_{p0} determines a much amplified underestimation on ρ_v and hence $\Delta Z = \rho_v/d$ extrapolated to lower frequencies. For example, at the selected field value $\mu_0 H = 0.5$ T, using ν_{p0} , $\chi = 0$ and the corresponding flux flow resistivity $1.4(1) \times 10^{-8} \Omega\text{m}$, through

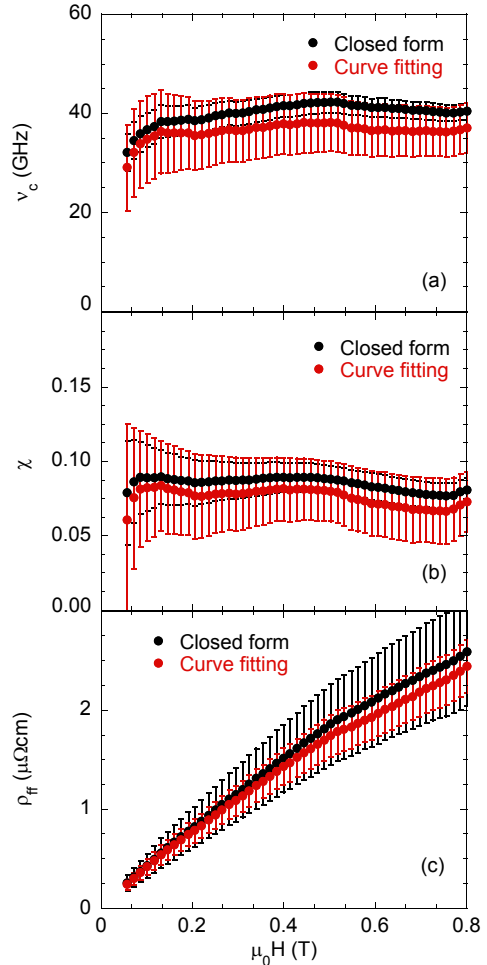


Fig. 8. (a) Characteristic frequency ν_c , (b) creep factor χ and (c) flux flow resistivity ρ_{ff} at $T = 10.00(5)$ K extracted from the measurements of ΔZ .

Eq. (1) $\Delta Z_{sim,0} = \rho_v/d$ vs the frequency ν can be numerically computed (here, the “sim” subscript highlights that the Z_{sim} is numerically computed, while the “0” subscript highlights that the computation is done for zero creep). Analogously, the reconstructed frequency dependence of $\Delta Z_{sim,\chi}$, where the “ χ ” subscript highlights that the experimentally obtained χ value is used, can be computed from the above reported values for ν_c and χ , and the corresponding $\rho_{ff} = 2.0(2) \times 10^{-8} \Omega\text{m}$. The results are reported in Fig. 9a, together with the relative discrepancies $\varepsilon_R := (R_{sim,\chi} - R_{sim,0})/R_{sim,\chi}$ and $\varepsilon_X := (X_{sim,\chi} - X_{sim,0})/X_{sim,\chi}$ in Fig. 9b. It can be seen that, in particular, the relative discrepancy on R can be as high as 100%, thus making the single frequency measurement completely unre-

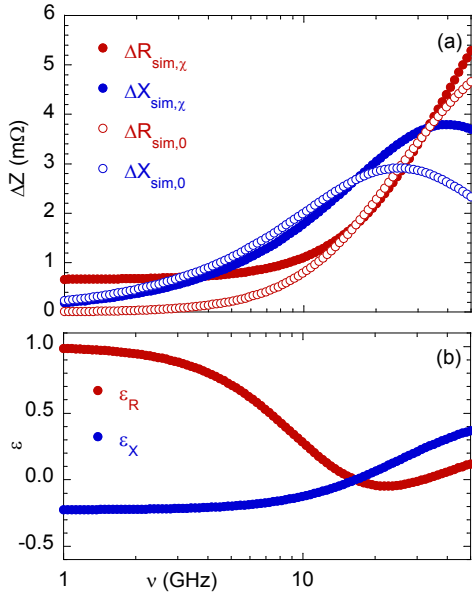


Fig. 9. Numerically computed ΔZ_{sim} – through Eq. (1) – at $\mu_0 H = 0.5$ T extrapolating the results of a dual frequency measurement (subscript “ χ ”) and single frequency measurement, (subscript “0”). Panel (a): ΔZ_{sim} vs frequency. Panel (b): relative discrepancies ε_R and ε_X , on ΔR_{sim} and ΔX_{sim} respectively, vs frequency.

liable in estimating the material behaviour at lower frequencies.

5. Summary

We have addressed the problem of a reliable extraction of the main parameters governing the complex resistivity ρ_ν and then the surface impedance of superconducting films in a dc magnetic field. We have recalled the main model for the high-frequency response, underlining the relevant role of the characteristic frequency ν_c in determining the response of a superconductor in a magnetic field. In fact, ν_c is a synthetic measure of the superconductor performance (the higher, the better). We have described and experimentally illustrated a dual mode resonator that can be used to measure ρ_ν on a superconducting thin film at two distinct frequencies to correctly extract the relevant vortex parameters, and in particular ν_c . We have quantitatively shown that routinely performed single frequency measurements of Z lead to heavy underestimations of ν_c and that the often neglected creep χ has to be taken

into account, together with an accurate determination of ν_c , to meaningfully extrapolate the Z frequency dependence. We have analysed the uncertainties resulting on the superconducting parameters, describing two alternative methods – namely, an analytical, closed form, approach and a standard curve fitting – to extract the mentioned quantities from the measurements. The advantages of both approaches have been highlighted, showing that the analytical one allows, in general, smaller uncertainties on ν_c and χ . Within this discussion, a general examination of the uncertainties attainable by the method in function of the possible frequency ranges of ν_c , and the subsequent criteria for its optimization, have been discussed. The results here presented are of relevance to design and optimize cutting-edge experiments, such as cavities for dark matter research, or for impressively large infrastructure, such as the beam screen of the Future Circular Collider, and for fundamental research.

6. Acknowledgments

Work partially supported by MIUR-PRIN project “HIBISCUS” - grant no. 201785KWLE. The authors warmly thank Giulia Sylva and Valeria Braccini at CNR-SPIN (Genova, Italy) for providing the FeSeTe sample.

Appendix A. Appendix

The explicit solution of the system of equations (7) is:

$$\frac{\nu_c}{\nu_1} = \frac{(p^2 - 1)\bar{r}_1\bar{r}_2 + \sqrt{\Lambda}}{2(p\bar{r}_1 - \bar{r}_2)} \quad (\text{A.1a})$$

$$\Lambda = \bar{r}_1^2\bar{r}_2^2(p^2 - 1)^2 - 4p(\bar{r}_2 - \bar{r}_1p)(p\bar{r}_2 - \bar{r}_1)$$

$$\chi = \frac{\frac{\nu_c}{\nu_i} - \bar{r}_i}{\frac{\nu_c}{\nu_i} \left(\frac{\nu_c}{\nu_i} \bar{r}_i + 1 \right)}, i = 1, 2 \quad (\text{A.1b})$$

where $p = \nu_2/\nu_1 > 1$. In the above, Eq. (A.1b) shows that, once ν_c is determined, χ can be indifferently computed through the two reported equivalent expressions. Moreover, the domain of the $\nu_c(\bar{r}_1, \bar{r}_2)$ function can be easily computed, yielding the result:

$$\frac{\bar{r}_1}{p} \leq \bar{r}_2 \leq p\bar{r}_1 \quad (\text{A.2})$$

After Eq.s(A.1), it is worth noting that the uncertainty on ν_c , $u(\nu_c)$:

$$u^2(\nu_c) = \sum_{i=1}^2 \left(\frac{\partial \nu_c}{\partial \bar{r}_i} \right)^2 \times \left(\frac{1}{\Delta r_i} \right)^2 (u^2(\Delta x_i) + \bar{r}_i^2 u^2(\Delta r_i)) \quad (\text{A.3})$$

can be evaluated in closed form from the experimentally measured quantities \bar{r}_i and from the evaluation of the four uncertainties $u(\Delta r_i)$ and $u(\Delta x_i)$. With the particularizations proposed in Sec. 3.5, Eq. (A.3) can be recast in the following:

$$u^2(\nu_c) = (u(\Delta r_1) G_1 d / \rho_{ff})^2 \times \sum_{i=1}^2 \left(\frac{\partial \nu_c}{\partial \bar{r}_i} \right)^2 (1 + \bar{r}_i^2) \left(\frac{1}{\rho_{v1,i}} \right)^2 s_i^2 \quad (\text{A.4})$$

where for compactness' sake, s_i has been introduced with $s_1 = 1$ and $s_2 = s$.

The expressions solving the system Eq. (7) for the flux flow resistivity are:

$$\rho_{ff,i} = G_i d \Delta r_i \frac{1 + \left(\frac{\nu_i}{\nu_c} \right)^2}{\chi + \left(\frac{\nu_i}{\nu_c} \right)^2} \quad (\text{A.5})$$

References

- [1] S. Posen, D. L. Hall, Nb₃Sn superconducting radiofrequency cavities: fabrication, results, properties, and prospects, *Supercond. Sci. Technol.* 30 (2017) 033004.
- [2] W. Cichalewski, J. Sekutowicz, A. Napieralski, R. Rybaniec, J. Branlard, V. Ayvazyan, Continuous Wave Operation of Superconducting Accelerating Cavities With High Loaded Quality Factor, *IEEE Trans. Nucl. Sci.* 67 (9) (2020) 2119–2127.
- [3] S. Calatroni, R. Vaglio, Surface Resistance of Superconductors in the Presence of a DC Magnetic Field: Frequency and Field Intensity Limits, *IEEE Trans. Appl. Supercond.* 27 (5) (2017) 3500506.
- [4] A. Abada, M. Abbrescia, S. S. AbdusSalam, I. Abdymukhanov, J. A. Fernandez, A. Abramov, M. Aburaia, A. O. Acar, P. R. Adzic, P. Agrawal, J. A. Aguilar-Saavedra, J. J. Aguilar-Verdugo, M. Aiba, I. Aichinger, G. Aielli, Etal, FCC-hh: The Hadron Collider. Future Circular Collider Conceptual Design Report Volume 3, *Eur. Phys. J. Spec. Top.* 228 (2019) 755–1107.
- [5] D. Alesini, C. Braggio, G. Carugno, N. Crescini, D. D. Agostino, D. Di Gioacchino, R. D. Vora, P. Falferi, S. Gallo, U. Gambardella, C. Gatti, G. Iannone, G. Lamanna, C. Ligi, A. Lombardi, R. Mezzena, A. Ortolan, R. Pengo, N. Pompeo, A. Rettaroli, G. Ruoso, E. Silva, C. C. Speake, L. Taffarello, S. Tocci, Galactic axions search with a superconducting resonant cavity, *Phys. Rev. D* 99 (2019) 101101(R).
- [6] D. Alesini, C. Braggio, G. Carugno, N. Crescini, D. D'Agostino, D. Di Gioacchino, R. Di Vora, P. Falferi, U. Gambardella, C. Gatti, G. Iannone, C. Ligi, A. Lombardi, G. Maccarrone, A. Ortolan, R. Pengo, C. Pira, A. Rettaroli, G. Ruoso, L. Taffarello, S. Tocci, High quality factor photonic cavity for dark matter axion searches, *Rev. Sci. Instrum.* 91 (9) (2020) 94701.
- [7] R. E. Collin, *Foundation for Microwave Engineering*, 2nd Edition, Singapore: McGraw-Hill International Editions, 1992.
- [8] L. D. Landau and E. M. Lifshits, *Physical Kinetics*, 2nd Edition, Pergamon Press, 1981.
- [9] J. D. Jackson, *Classical Electrodynamics*, 3rd Edition, John Wiley & Sons Inc., USA, 1999.
- [10] N. Pompeo, K. Torokhtii, E. Silva, Surface impedance measurements in thin conducting films: Substrate and finite-thickness-induced uncertainties, in: *Proc. IEEE Int. Instrum. Meas. Technol. Conf.* 22–25 May Turin Italy, no. 3, 2017, pp. 1–5.
- [11] M. Tinkham, *Introduction to Superconductivity*, 2nd Edition, McGraw-Hill, Inc., New York, NY, USA, 1996.
- [12] M. Golosovsky, M. Tsindlekht, D. Davidov, High-frequency vortex dynamics in YBa₂Cu₃O₇, *Supercond. Sci. Technol.* 9 (1) (1996) 1–15.
- [13] N. Pompeo, A. Alimenti, K. Torokhtii, E. Silva, Physics of vortex motion by means of microwave surface impedance measurements (Review article), *Low Temp. Phys.* 46 (4) (2020) 343–347.
- [14] N. Pompeo, E. Silva, Reliable determination of vortex parameters from measurements of the microwave complex resistivity, *Phys. Rev. B* 78 (9) (2008) 094503.
- [15] J. I. Gittleman, B. Rosenblum, Radio-frequency resistance in the mixed state for subcritical currents, *Phys. Rev. Lett.* 16 (17) (1966) 734–736.
- [16] C. Song, T. Heitmann, M. DeFeo, K. Yu, R. McDermott, M. Neeley, J. M. Martinis, B. Plourde, Microwave response of vortices in superconducting thin films of Re and Al, *Phys. Rev. B* 79 (17) (2009) 174512.
- [17] E. Silva, N. Pompeo, S. Sarti, Wideband microwave measurements in Nb/Pd₈₄Ni₁₆/Nb structures and comparison with thin Nb films, *Supercond. Sci. Technol.* 24 (2) (2011) 24018.
- [18] E. Silva, N. Pompeo, K. Torokhtii, S. Sarti, Wideband Surface Impedance Measurements in Superconducting Films, *IEEE Trans. Instrum. Meas.* 65 (5) (2016) 1120–1129.
- [19] J. C. Booth, D. H. Wu, S. M. Anlage, A broadband method for the measurement of the surface impedance of thin films at microwave frequencies, *Rev. Sci. Instrum.* 65 (6) (1994) 2082–2090.
- [20] H. Kitano, T. Ohashi, A. Maeda, Broadband method for precise microwave spectroscopy of superconducting thin films near the critical temperature., *Rev. Sci. Instrum.* 79 (7) (2008) 074701.
- [21] M. M. Felger, M. Dressel, M. Scheffler, Microwave resonances in dielectric samples probed in Corbino geometry: Simulation and experiment, *Rev. Sci. Instrum.* 84 (2013) 114703.
- [22] Y. Kobayashi, H. Yoshikawa, Microwave measurements of surface impedance of high-T_c superconductors using two modes in a dielectric rod resonator, *IEEE Trans. Microw. Theory Tech.* 46 (12) (1998) 2524–2530.
- [23] M. V. Jacob, J. Mazierska, K. Leong, J. Krupka, Simplified Method for Measurements and Calculations of Coupling Coefficients and Q o Factor of High-Temperature

- Superconducting Dielectric Resonators, *IEEE Trans. Microw. Theory Tech.* 49 (12) (2001) 2401–2407.
- [24] H.-t. Lue, J.-t. Lue, T.-y. Tseng, Microwave Penetration Depth Measurement for High Tc Superconductors by Dielectric Resonators, *IEEE Trans. Instrum. Meas.* 51 (3) (2002) 433–439.
- [25] N. Cherpak, S. Member, A. Barannik, Y. Filipov, Y. Prokopenko, S. Vitusevich, Accurate Microwave Technique of Surface Resistance Measurement of Large-Area HTS Films Using Sapphire Quasi-Optical Resonator, *IEEE Trans. Appl. Supercond.* 13 (2) (2003) 3570–3573.
- [26] T. Hanaguri, K. Takaki, Y. Tsuchiya, A. Maeda, An instrument for low- and variable-temperature millimeter-wave surface impedance measurements under magnetic fields, *Rev. Sci. Instrum.* 74 (10) (2003) 4436–4441.
- [27] T. Hashimoto and Y. Kobayashi, Frequency Dependence Measurements of Surface Resistance of Superconductors Using Four Modes in a Sapphire Rod Resonator, *IEICE Trans. Electron.* E86-C (8) (2003) 1721–1728.
- [28] N. Cherpak, A. Barannik, S. Bunyaev, Y. Prokopenko, S. Vitusevich, Measurements of Millimeter-Wave Surface Resistance and Temperature Dependence of Reactance of Thin HTS Films Using Quasi-Optical Dielectric Resonator, *IEEE Trans. Appl. Supercond.* 15 (2) (2005) 2919–2922.
- [29] G. Ghigo, D. Andreone, D. Botta, A. Chiodoni, R. Gerbaldo, L. Gozzelino, F. Laviano, B. Minetti, E. Mezzetti, Non-uniform columnar defect implantation in YBCO coplanar resonators for the control of vortex-induced microwave dissipation and nonlinearity, *Supercond. Sci. Technol.* 18 (2005) 193–199.
- [30] W. A. Huttema, B. Morgan, P. J. Turner, W. N. Hardy, X. Zhou, D. A. Bonn, R. Liang, D. M. Broun, Apparatus for high-resolution microwave spectroscopy in strong magnetic fields, *Rev. Sci. Instrum.* 77 (2) (2006) 023901.
- [31] J.-h. Yeh, S. M. Anlage, In situ broadband cryogenic calibration for two-port superconducting microwave resonators, *Rev. Sci. Instrum.* 84 (2013) 034706 1–8.
- [32] N. Pompeo, K. Torokhtii, E. Silva, Dielectric Resonators for the Measurements of the Surface Impedance of Superconducting Films, *Meas. Sci. Rev.* 14 (3) (2014) 164–170.
- [33] S. Ohshima, N. Takanashi, A. Saito, K. Nakajima, T. Nagayama, Effect of Si-Ion Irradiation on Microwave Surface Resistance in YBa₂Cu₃O_y Thin Films in Magnetic Fields, *IEEE Trans. Appl. Supercond.* 28 (4) (2018) 1–4.
- [34] A. Alimenti, K. Torokhtii, E. Silva, N. Pompeo, Challenging microwave resonant measurement techniques for conducting material characterization, *Meas. Sci. Technol.* 30 (2019) 065601.
- [35] International Electrotechnical Commission, IEC 61788-7:2020 Superconductivity - Part 7: Electronic characteristic measurements - Surface resistance of high-temperature superconductors at microwave frequencies (2020).
- [36] J. Powell, A. Porch, R. Humphreys, F. Wellhöfer, M. Lancaster, C. Gough, Field, temperature, and frequency dependence of the surface impedance of YBa₂Cu₃O₇ thin films, *Phys. Rev. B* 57 (9) (1998) 5474–5484.
- [37] B. W. Hakki and P. D. Coleman, A Dielectric Resonator Method of Measuring Inductive Capacities in the Millimeter Range, *IRE Trans. Microw. Theory Tech.* 8 (4) (1960) 402–410.
- [38] N. Pompeo, K. Torokhtii, A. Alimenti, E. Silva, Dual frequency resonator for the correct determination of the in-field surface impedance frequency dependence of superconductors, in: 24th IMEKO TC4 Int. Symp., 2020, pp. 75–79.
- [39] N. Pompeo, K. Torokhtii, and E. Silva, Design and test of a microwave resonator for the measurement of resistivity anisotropy, *Measurement* 98 (2017), 414–420.
- [40] N. Pompeo, K. Torokhtii, F. Leccese, A. Scorza, S. Scuito, E. Silva, Fitting strategy of resonance curves from microwave resonators with non-idealities, in: *Proc. IEEE Int. Instrum. Meas. Technol. Conf.* 22–25 May Turin Italy, Vol. 21, 2017, pp. 1–6.
- [41] K. Torokhtii, A. Alimenti, N. Pompeo, E. Silva, Uncertainty in uncalibrated microwave resonant measurements, in: 24th IMEKO TC4 Int. Symp., 2019, pp. 1–5.
- [42] D. H. Staelin, A. W. Morgenthaler, J. A. Kong, *Electromagnetic Waves*, Prentice-Hall, Inc., 1994.
- [43] M. Žic, An alternative approach to solve complex nonlinear least-squares problems, *J. Electroanal. Chem.* 760 (2016) 85–96.
- [44] J. J. More, B. S. Garbow, K. E. Hillstom, User guide for MINPACK-1. [In FORTRAN], Tech. rep., United States (1980).
- [45] V. Braccini, S. Kawale, E. Reich, E. Bellingeri, L. Pellegrino, A. Sala, M. Putti, K. Higashikawa, T. Kiss, B. Holzapfel, C. Ferdeghini, Highly effective and isotropic pinning in epitaxial Fe(Se,Te) thin films grown on CaF₂ substrates, *Appl. Phys. Lett.* 103 (2013) 172601.
- [46] N. Pompeo, K. Torokhtii, A. Alimenti, G. Sylva, V. Braccini, E. Silva, Pinning properties of FeSeTe thin film through multifrequency measurements of the surface impedance, *Supercond. Sci. Technol.* 33 (11) (2020) 114006.
- [47] K. Torokhtii, A. Alimenti, F. Rizzo, A. Augieri, G. Celentano, A. Frolova, E. Silva, N. Pompeo, High frequency vortex dynamics in YBa₂Cu₃O_{7-x} with Ba₂YTaO₆-Ba₂YNbO₆ nanodefects, *J. Phys. Conf. Ser.* 1559 (2020) 12043.
- [48] J. Krupka, K. Derzakowski, B. Riddle, J. Baker-Jarvis, A dielectric resonator for measurements of complex permittivity of low loss dielectric materials as a function of temperature, *Meas. Sci. Technol.* 9 (10) (1998) 1751–1756.
- [49] J. Krupka, K. Derzakowski, M. Tobar, J. Hartnett, R. G. Geyer, Complex permittivity of some ultralow loss dielectric crystals at cryogenic temperatures, *Meas. Sci. Technol.* 10 (5) (1999) 387–392.
- [50] M. Bienias, S. Gao, K. Hasche, R. Seemann, K. Thiele, A metrological scanning force microscope used for coating thickness and other topographical measurements, *Appl. Phys. A* 66 (1) (1998) S837–S842.
- [51] D.-H. Wu, J. Booth, S. Anlage, Frequency and field Variation of Vortex Dynamics in YBa₂Cu₃O_{7-δ}, *Phys. Rev. Lett.* 75 (3) (1995) 525–528.
- [52] J. Bardeen, M. Stephen, Theory of the Motion of Vortices in Superconductors, *Phys. Rev.* 140 (4A) (1965) 1197–1207.
- [53] N. Pompeo, A. Alimenti, K. Torokhtii, G. Sylva, V. Braccini, E. Silva, Microwave properties of Fe(Se,Te) thin films in a magnetic field: pinning and flux flow, *J.*

Phys. Conf. Ser. 1559 (2020) 012055.

- [54] T. Okada, F. Nabeshima, H. Takahashi, Y. Imai, A. Maeda, Exceptional Suppression of Flux-Flow Resistivity in $\text{FeSe}_{0.4}\text{Te}_{0.6}$ by Back-Flow from Excess Fe Atoms and Se/Te Substitutions, Phys. Rev. B 91 (2015) 054510.